Icarus **147**, 520–529 (2000)
doi:10.1006/icar.2000.6470, available online at http://www.idealibrary.com on IDEAL®

# Radar Observations of Asteroid 2100 Ra-Shalom

Michael K. Shepard

*Department of Geography and Geosciences, Bloomsburg University, Bloomsburg, Pennsylvania 17815*
E-mail: mshepard@bloomu.edu

Lance A. M. Benner, Steven J. Ostro, Alan W. Harris, and Keith D. Rosema[1]

*Jet Propulsion Laboratory, California Institute of Technology, Pasadena, California 91109*

Irwin I. Shapiro and John F. Chandler

*Harvard–Smithsonian Center for Astrophysics, Cambridge, Massachusetts 02138*

and

Donald B. Campbell

*National Astronomy and Ionosphere Center, Cornell University, Ithaca, New York 14853*

Received February 29, 2000; revised June 2, 2000

**We report Doppler-only (cw) radar observations of near-Earth Asteroid 2100 Ra-Shalom obtained at the Arecibo Observatory using a transmitter frequency of 2380 MHz (12.6 cm) on 1984 Aug. 18–22. Weighted and filtered sums of cw echoes achieve a maximum signal-to-noise ratio of 74 and cover the asteroid in rotation phase. A weighted sum of all cw spectra gives an opposite circular (OC) radar cross section of $1.13 \pm 0.40$ km$^2$ and a circular polarization ratio of $0.31 \pm 0.02$. Inversion of echo edge frequencies yields a convex hull with an elongation (maximum breadth/minimum breadth) of $1.15 \pm 0.03$ and places a lower bound on the maximum pole-on dimension of 2.4 km/cos $\delta$, where $\delta$ is the angle between the radar line-of-sight and the asteroid's apparent equator. Ra-Shalom has one of the least elongated pole-on silhouettes of the near-Earth asteroids for which similar shape information from radar observations is available. Ra-Shalom's effective diameter (diameter of a sphere with equal cross-sectional area) is constrained to a range of 2.4–3.6 km. We use a two-component radar scattering model to remove the "diffuse" contributions from Ra-Shalom's radar cross section and obtain a surface bulk density estimate of 1.1–3.3 g cm$^{-3}$. When compared with reported bulk densities and porosities of meteorites, our results are consistent with either: (1) a C-class asteroid with carbonaceous-chondritic composition, effective diameter 2.6–3.6 km, and surface porosity <70%; or (2) an S-class asteroid with ordinary-chondritic or stony-iron composition, effective diameter 2.4–2.6 km, and little or no surface regolith. Ra-Shalom's near-surface roughness appears to be globally heterogeneous.** 

*Key Words:* **asteroids; radar; surfaces, asteroids; asteroids, composition; asteroids, Ra-Shalom.**

## INTRODUCTION

2100 Ra-Shalom, one of 77 known Aten asteroids (as of May 2000), was discovered on 1978 September 10 by Helin *et al.* (1978). Shortly after its discovery, Lebofsky *et al.* (1979) obtained radiometry, polarimetry, and UBV photometry and classified Ra-Shalom as a C-type asteroid with a high surface thermal inertia. Additional observations and modeling have supported the high surface thermal inertia interpretation (Veeder *et al.* 1989, Harris *et al.* 1998), but the C classification has been questioned (Harris *et al.* 1998). Estimated physical properties of Ra-Shalom are listed in Tables I and II.

Ostro *et al.* (1984) conducted radar observations of Ra-Shalom at Arecibo (12.6-cm wavelength) on 1981 Aug. 23–26. They concluded that their data were consistent with the asteroid having a largest dimension near 3 km and a somewhat irregular shape. They found the echo bandwidth to be within about 1.5 Hz of 5.0 Hz on each date, but their estimates of radar properties varied widely from night to night: unweighted opposite circular radar cross section $\sigma_{OC} = 0.59 \pm 0.35$ km$^2$ and circular polarization ratio $\mu_C = 0.20 \pm 0.07$ (uncertainties are rms dispersions about the mean).

Here we report radar observations of Ra-Shalom in 1984 with an Arecibo system (12.6-cm wavelength, transmitter power $\sim$420 KW, antenna gain $\sim 10^7$) that was more sensitive and much

[1] Present address: 5209 21st Avenue NE, Seattle, Washington 98105.



0019-1035/00 $35.00

**TABLE I**
**Estimated Physical Properties**

| Property | Value |
|---|---|
| $H$ (mag) | $16.07 \pm 0.08$[a] |
| Class | C,[b] S?[c] |
| $P$ (h) | $19.797 \pm 0.003$[a] |
| | 19.79[d] |
| $\Delta m$ (mag) | 0.41[a] |
| $\Gamma$(erg cm$^{-2}$ s$^{-0.5}$ K$^{-1}$) | $\geq 1.1 \times 10^6$ [c] |

*Note.* $H$ is the absolute visual magnitude, class refers to the taxonomic class, $P$ is the synodic rotation period, $\Delta m$ indicates the observed range of the lightcurve amplitude, and $\Gamma$ is the surface thermal inertia.
[a] Pravec *et al.* (1998).
[b] McFadden *et al.* (1984).
[c] Harris *et al.* (1998).
[d] Ostro *et al.* (1984).

better calibrated than that available in 1981. In particular, in 1984 we used a dual-polarization receiver, while in 1981 the receiver had to be switched back and forth between the same circular (SC) and opposite circular (OC) polarizations to that of the transmission. The OC cross sections measured on 1981 Aug. 23–25 were significantly smaller than that measured on 1981 Aug. 26. Our 1984 Aug. 18–22 OC cross sections are consistent with each other and with the 1981 Aug. 26 value, suggesting that the 1981 Aug. 23–25 calibration was faulty, possibly due to undocumented pointing errors in the instrumentation. The asteroid's 19.79-h spin period, suspected by Ostro *et al.* 1984, has since been confirmed (Pravec *et al.* 1998), and we use this value in our analysis.

**TABLE II**
**Size Estimates**

| $D_{\rm eff}$ (km) | $p_{\rm v}$ | Technique |
|---|---|---|
| 1.7 | 0.16 | IR STM[a] |
| 1.72 | 0.26 | IR STM[b] |
| $2.04 \pm 0.10$ | $0.115 \pm 0.010$ | IR STM[c] |
| 2.4 | 0.08 | IR FRM[a] |
| 2.64 | 0.11 | IR FRM[b] |
| $3.42 \pm 0.18$ | $0.04 \pm 0.004$ | IR FRM[c] |
| 2.48 km | 0.13 | IR NEATM[b] |
| $D_{\rm max} \geq 2.40$ km | 0.05 – 0.13 | Radar (this work) |
| $D_{\rm max} \geq 2.9$ km | — | Radar[d] |
| 3.56 km | (0.037) | Polarimetry[c] |

*Note.* $D_{\rm eff}$ is the diameter of a sphere with equal cross-sectional area. Radar-based diameters are lower bounds on the maximum diameter. Visual albedo ($p_{\rm v}$) estimates were calculated (by their respective authors) based on their associated diameters and the best absolute magnitude estimates available at the time of each study. IR indicates that infrared radiometry was used; STM is the "standard thermal model;" FRM is the "fast rotating model;" and NEATM is the "near-Earth asteroid thermal model" (cf. Refs. *b* and *c*). The polarimetric diameter estimate (Ref. *c*) was based on the assumption of the albedo in parentheses. Uncertainties have been given where available.
[a] Veeder *et al.* (1989).
[b] Harris *et al.* (1998).
[c] Lebofsky *et al.* (1979).
[d] Ostro *et al.* (1984).

**TABLE III**
**Observations**

| Date | RA (°) | DEC (°) | Distance (AU) | Runs | Receive start–stop (UTC hrs) | $\phi$ (°) |
|---|---|---|---|---|---|---|
| 1984 Aug 18 | 268 | 28 | 0.206 | 22 | 19.23–21.73 | 0–45 |
| 1984 Aug 19 | 269 | 26 | 0.209 | 17 | 19.19–21.75 | 76–121 |
| 1984 Aug 20 | 269 | 24 | 0.213 | 24 | 19.06–21.83 | 150–199 |
| 1984 Aug 21 | 270 | 22 | 0.216 | 24 | 19.06–21.80 | 226–275 |
| 1984 Aug 22 | 271 | 20 | 0.220 | 21 | 19.19–21.83 | 305–352 |

*Note.* Right ascension, declination, and distance are given at the beginning of each day's observations. "Runs" refers to the number of transmit–receive cycles. $\phi$ is the range in rotation phase covered on each day, arbitrarily set to 0° for the first reception on the first day and based on a rotation period of 19.79 h. The frequency resolution of each run was 0.098 Hz.

Our basic data-acquisition and reduction techniques were similar to those described most recently by Mitchell *et al.* (1995). Table III gives ephemeris information and the number of transmit–receive cycles (runs) completed on each date.

## RESULTS

Figure 1 shows weighted sums of echo power spectra from each day. There was no overlap in the day-to-day rotation-phase coverage. Calibration uncertainties in these data are systematic and can be considered a constant source of error in all measurements; we estimate these to be ±35% for this experiment and due primarily to uncertainties in pointing and antenna gain. Uncertainties due to random noise vary from ∼2–4% in the daily sums shown in Fig. 1. Our estimates of the asteroid's disc-integrated radar properties show day-to-day variations that are larger than our expected uncertainties and are therefore probably physically significant (Table IV). There also appear to be positive correlations between bandwidth, radar cross section, and circular polarization ratio, which are discussed at greater length below.

The mean OC radar cross section and circular polarization ratio for the entire experiment are $\sigma_{\rm OC} = 1.13 \pm 0.40$ km$^2$ and $\mu_{\rm C} = 0.31 \pm 0.02$, respectively. Among the 16 C-class main-belt and near-Earth asteroid (NEA) radar detections previously reported, the circular polarization ratio of Ra-Shalom is greater than those for 14, comparable to that for 1, and less than that for 1, indicating that its near surface is significantly rougher at decimeter scales than the average radar-detected C-class asteroid.

Figure 2 shows sums of spectra sorted by rotation phase. Echoes are not readily detected in some of the spectra because of gaps in coverage and/or low system sensitivity.

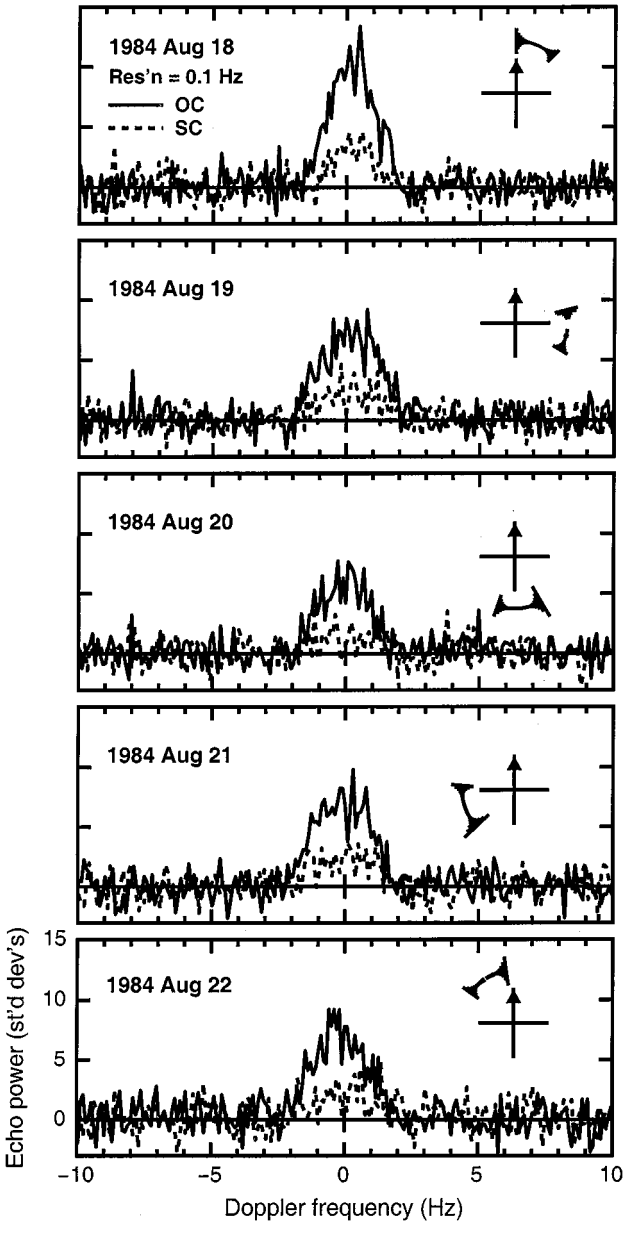


**FIG. 1.** Weighted (by SNR) sums of echo power spectra of Ra-Shalom, grouped by observation date. Insets indicate relative rotational phase coverage; 0° is arbitrarily assigned to the beginning of reception during the first run on 1984 Aug 18 19.23 UTC. The lengths of the radial line segments at each phase are proportional to the noise level. A vertical bar at 0 Hz indicates 1 standard deviation ($\sigma$) of the OC receiver noise.

## PHYSICAL PROPERTIES

### *Hull Estimation*

Given sufficient rotational coverage and echo strength, measurements of echo edge frequencies can be used to obtain the convex hull of the target's pole-on silhouette (Ostro *et al.* 1988, 1990). The convex hull can be thought of as the shape of a rubber band stretched around the pole-on silhouette of the asteroid. As discussed by Ostro *et al.* (1988), the accuracy of hull estimation depends on the frequency and rotation-phase resolution of the spectra and the ability to discern the spectral edges of the echoes, which depends strongly upon the signal-to-noise ratio (SNR). For this data set, the rotational coverage and signal-to-noise ratio are near the lower limit of what is necessary for the computation of a hull. The largest gap in phase coverage (modulo 180°) is approximately 5°. (The determination of the hull silhouette requires only 180° of contiguous phase coverage; therefore, all discussions of phase coverage or gaps are modulo 180°.) We arbitrarily chose the first return echo from the first run to be 0° rotation phase. A significant number of individual runs had very low SNRs, making spectral edge detection difficult or impossible. Because of this, we smoothed all runs using a 1-Hz frequency filter, and then excluded 35 runs in which SNRs were less than $4\sigma$ leaving 73 of the original 108. The resulting phase coverage, despite three $\sim$14° gaps, is still adequate for hull estimation. *Unless otherwise stated in the following, the uncertainties quoted span the full range of those values observed.*

We estimated the hull using the OC spectra as follows. We smoothed the spectra to frequency resolutions of 0.3, 0.4, 0.5, 0.75, and 1.0 Hz, and for each frequency resolution we smoothed the spectra to phase resolutions of 5°, 10°, and 15°. To each of these 15 data sets, we added a synthetic echo spectrum for a Lambertian sphere with the same radar cross section and bandwidth as those of the asteroid at each of five different center frequencies that did not overlap echoes from the asteroid, thus contaminating the synthetic (model) spectra with noise. For each of the five synthetic spectra, we estimated the hull, using edge-frequency detection thresholds between 0 and 2 standard deviations in intervals of 0.1 standard deviation. Because no single combination of frequency/phase smoothing and threshold estimators perfectly estimated the model hull, we chose five combinations that best reproduced the circular shape (using the breadth

**TABLE IV**
**Disc-Integrated Radar Properties**

| Date | OC SNR | $B$ (Hz) | $\sigma_{oc}$ (km$^2$) | $\mu_c$ |
|---|---|---|---|---|
| 1984 Aug 18 | 42 | $3.0+0.3/-0.6$ | $1.16\pm0.03$ | $0.27\pm0.02$ |
| 1984 Aug 19 | 33 | $3.2+0.5/-0.2$ | $1.35\pm0.04$ | $0.35\pm0.03$ |
| 1984 Aug 20 | 26 | $2.5+0.4/-0.7$ | $0.82\pm0.03$ | $0.21\pm0.02$ |
| 1984 Aug 21 | 33 | $3.1+0.3/-0.1$ | $1.15\pm0.03$ | $0.28\pm0.02$ |
| 1984 Aug 22 | 32 | $2.8+0.7/-0.4$ | $1.26\pm0.04$ | $0.38\pm0.03$ |
| Whole experiment | 74 | $3.5+0.4/-0.2$ | $1.13\pm0.02$ | $0.31\pm0.02$ |

*Note.* Radar properties on each date were determined from weighted (by SNR) sums of cw spectra. OC SNR is the OC signal-to-noise ratio obtained from an optimally filtered weighted spectral sum. $B$ is bandwidth estimated from the spectral edges at the $2\sigma$ noise level. $\sigma_{OC}$ is the OC radar cross section and $\mu_C$ is the circular polarization ratio. Uncertainties in $B$ are based on the bandwidth difference observed when estimating spectral edges at the 1- and $3\sigma$ crossing points. Uncertainties quoted for $\sigma_{OC}$ and $\mu_C$ are $1\sigma$ standard errors caused by background noise. Absolute (calibration) uncertainties in $\sigma_{OC}$ are estimated to be $\pm$35%.

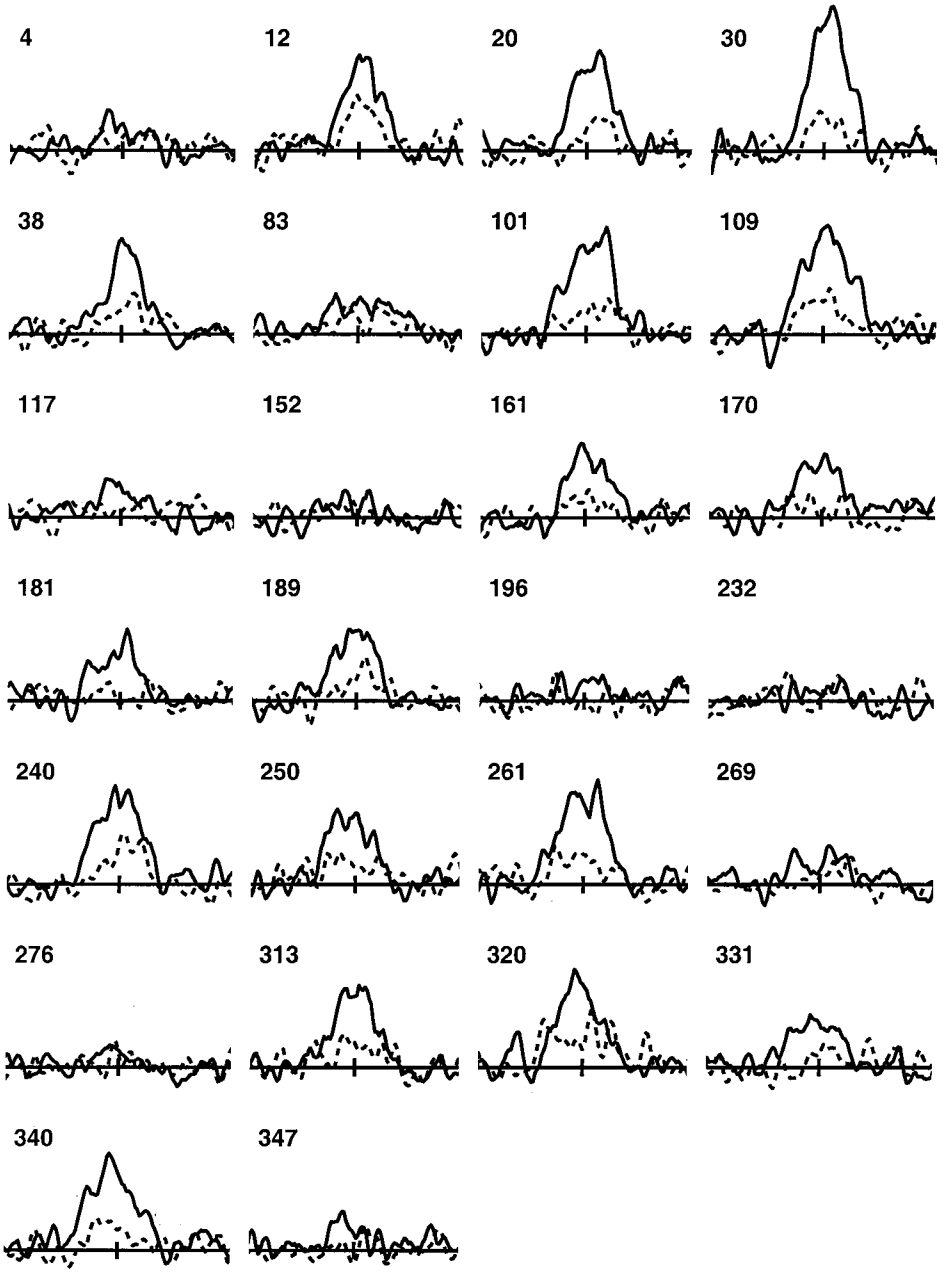


**FIG. 2.** Weighted summed spectra within 10° phase intervals and smoothed to 0.5 Hz resolution. Labels give the weighted mean rotation phase in degrees. Identical linear scales are used throughout the figure. Each horizontal axis extends from −5 Hz on the left to +5 Hz on the right. A vertical bar at 0 Hz indicates ±1 standard deviation of the OC receiver noise. Each plot may represent as many as five summed spectra. Particularly low SNRs (e.g., plots at 152°, 196°, and 276° phase) are due to low numbers of summed spectra (as few as one) and/or low individual run SNR. Gaps in phase indicate a lack of observations.

ratio as a proxy—see below) and correct bandwidth of the model Lambert sphere (Table V). Figure 3 shows the estimates of the Lambert model's hull obtained using those combinations. The scatter of the hulls about the model conveys the degree of uncertainty that may be expected from our Ra-Shalom hull estimate using those combinations. A simple measure of hull circularity is the breadth (or aspect) ratio (BR) of the hull's maximum to minimum widths. A circular hull (as well as several other equant, but noncircular figures) has a BR equal to 1. The mean BR and bandwidth for the 25 estimates (five synthetic spectra, five hull estimates each) of the Lambert model are $1.14 + 0.08/-0.07$ and $3.801 \pm 0.458$ Hz, respectively. We underestimate the actual model bandwidth (3.908 Hz) by $3 \pm 12\%$.

Next, we applied the same filtering/threshold combinations to estimate Ra-Shalom's hull. We repeated this process for a large enough range of center frequency values to locate the asteroid's center-of-mass (COM), given by the minimum value of the weighted sum of squares of the residuals ($\chi^2$). Figure 4 overlays

**TABLE V**
**Hull Estimators**

| Phase resolution (°) | Frequency resolution (Hz) | Edge detection threshold (st. dev.'s of noise) |
|---|---|---|
| 5.0 | 0.50 | 0.4 |
| 5.0 | 0.75 | 0.9 |
| 10.0 | 0.50 | 0.7 |
| 15.0 | 0.40 | 0.7 |
| 15.0 | 0.50 | 0.9 |

estimates of Ra-Shalom's hull obtained with the five estimators. The five are consistent in shape with a mean BR of $1.15 + 0.03/-0.02$, and a mean bandwidth of $3.67 + 0.35/-0.31$ Hz. Ra-Shalom has among the least elongated pole-on silhouettes of any NEA for which similar shape information from radar data is available. Elongations have been reported for 12 other radar-detected NEAs; their mean and standard deviation is $1.6 \pm 0.4$, with a (previous) minimum of 1.18 (1991 CS) and maximum of 2.5 (1620 Geographos) (Benner *et al.* 1999, Hudson and Ostro 1999).

*Size*

We adopt 3.36 Hz, our lowest bandwidth estimated above, as a lower bound on the maximum breadth of Ra-Shalom's pole-on silhouette. Using the known rotation period of 19.79 h, this corresponds to a maximum pole-on breadth, $D_{\max}$, of 2.40 km/cos $\delta$, where $\delta$ is the subradar latitude. There are several estimates of Ra-Shalom's size reported in the literature (Table II) with effective diameters (the diameter of a sphere with equivalent cross-sectional area), $D_{\text{eff}}$, ranging from 1.7 to 3.6 km. The sizes obtained by us and by Ostro *et al.* (1984) are *lower* bounds on $D_{\max}$. The highest estimates in Table II (3.56 and $3.42 \pm 0.18$ km) were based on polarimetry and radiometry, respectively. The lowest estimates were all based upon the application of the "standard thermal model" (STM) to radiometric observations of Ra-Shalom (cf. Lebofsky and Spencer 1989) which assumes a nonrotating asteroid, zero thermal inertia surface (e.g., fine-grained or "dusty" regolith), and thermal emission only from the Sun-facing hemisphere. However, the STM does a poor job of fitting Ra-Shalom's radiometric observations and the consensus is that its surface has a high thermal inertia consistent with bare rock, or a very thin (less than a few centimeters) regolith overlying a solid substrate (Lebofsky *et al.* 1979, Veeder *et al.* 1989, Harris *et al.* 1998). Harris *et al.* 1998 note that the lunar regolith has a thermal inertia, $\Gamma \sim 5 \times 10^4$ erg cm$^{-2}$ s$^{-0.5}$ K$^{-1}$, at least a factor of 20 lower than their estimate for Ra-Shalom (Table I). We therefore exclude the estimates based on the STM and adopt 2.4–3.6 km as the most likely range of $D_{\text{eff}}$ for Ra-Shalom.

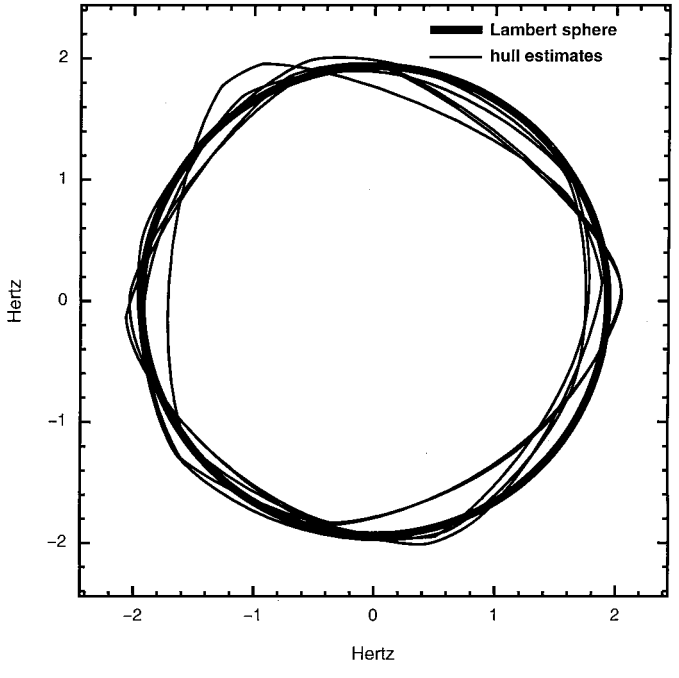


**FIG. 3.** Estimates of a Lambert sphere's hull from synthetic spectra contaminated with noise. Five estimators are shown (thin lines), corresponding to one realization of noise and five different phase/frequency/threshold combinations (Table V). The dispersion of the hulls about the circle (the model's actual hull) give a visual sense of the uncertainties that are present in our estimates of Ra-Shalom's hull.

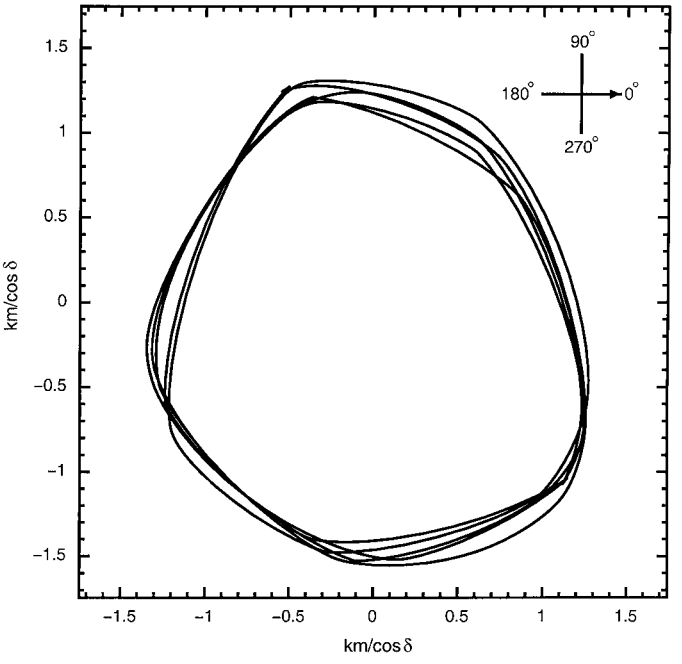


**FIG. 4.** Estimates of Ra-Shalom's hull, using the five phase/frequency/threshold combinations given in Table V. Rotation phase orientation for the plot is shown with an inset cross.

*Classification*

Figure 5 shows how the radar and optical albedos of Ra-Shalom depend on its effective diameter. The radar albedo is

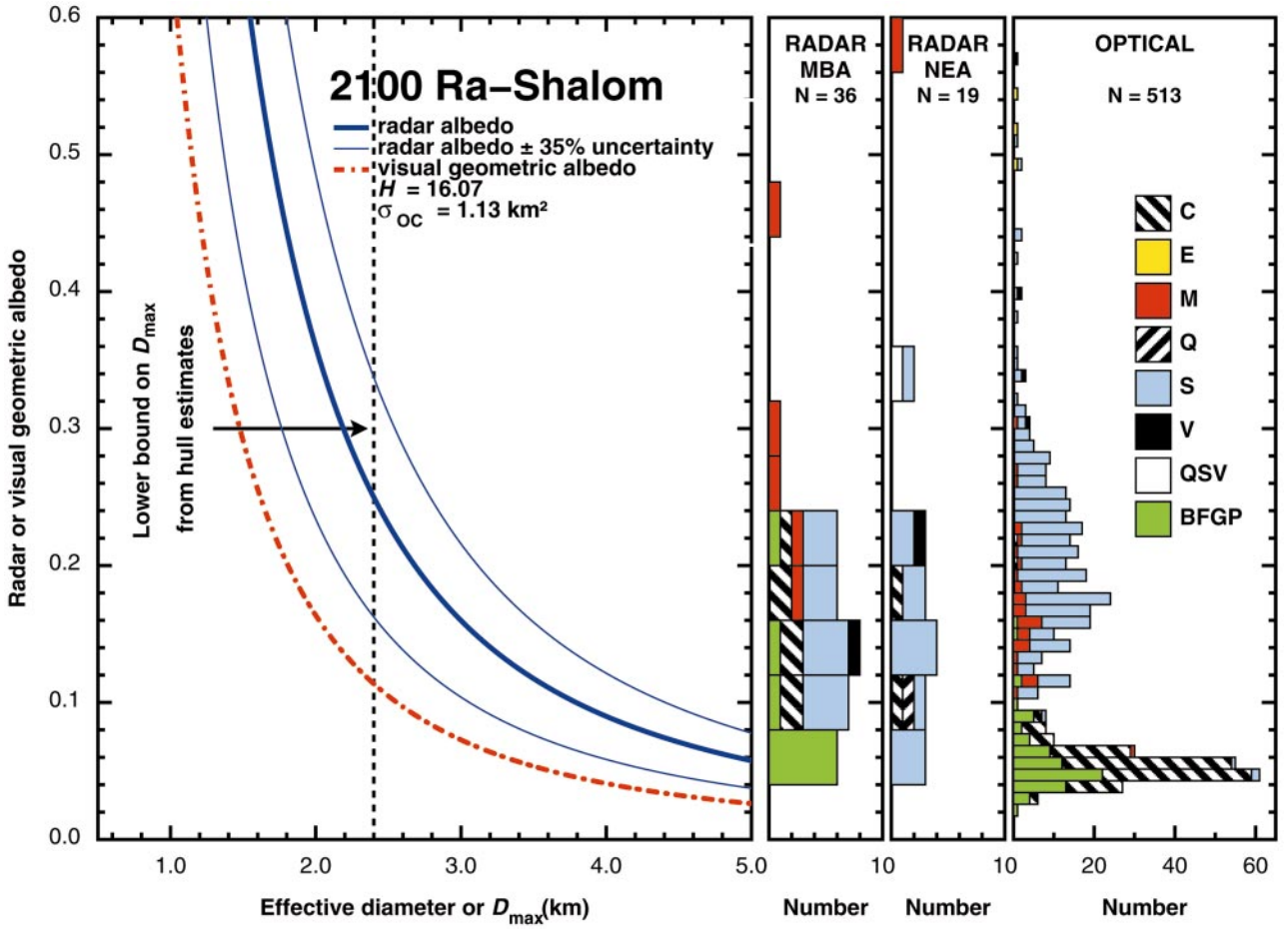


**FIG. 5.** Constraints on Ra-Shalom's diameter, radar albedo, and visual geometric (or optical) albedo. Radar albedo is shown as a thick solid curve computed using Ra-Shalom's OC radar cross section (Table IV). Thin solid curves denote the $1\sigma$ uncertainty in the radar albedo that propagates from the 35% uncertainty in $\sigma_{OC}$. Allowed geometric albedos, shown as the dash–dot curve, were computed as a function of diameter from $\log p_v = 6.259 - 2\log D - 0.4H$ (Bowell *et al.* 1989), where $H$ is Ra-Shalom's absolute magnitude (Table I). The vertical dashed line denotes a lower bound on the pole-on breadth from the hull estimation. Histograms show the distribution by taxonomic class of main-belt (Magri *et al.* 1999) and near-Earth asteroids, and radar and optical albedos (optical albedos were taken from the JPL/Horizons online data base: http://ssd.jpl.nasa.gov/horizons.html, Chamberlin *et al.* 1997).

defined as

$$\hat{\sigma}_{OC} = \frac{4\sigma_{OC}}{\pi D_{eff}^2}.$$

Figure 5 also indicates representative values of the optical geometric albedo, $p_v$, for principal taxonomic classes, and it condenses information about the distribution of estimates of other asteroid radar albedos. Using the range of sizes discussed above, we infer that the radar cross section and absolute magnitude of Ra-Shalom correspond to limits on the radar and optical albedos of $0.07 < \hat{\sigma}_{OC} < 0.33$ and $0.05 < p_v < 0.13$. Both ranges span values consistent with Ra-Shalom's C-class taxonomy. Based on the range of radar albedo alone, we cannot exclude any classification for Ra-Shalom (Magri *et al.* 1999), but using our adopted size constraints and associated range of optical albedo, we can safely rule out higher albedo classes E and V as too bright. There are two other high albedo classes not shown explicitly in Fig. 5, A and R, which can also be excluded from further consideration (Tedesco *et al.* 1984, Tholen and Barucci 1984).

### *Astrometry*

Our hull estimation yields an estimate, $-98091.66 \pm 0.12$ Hz, for the Doppler frequency corresponding to Arecibo echoes from Ra-Shalom's COM at 00:00:00 UTC on 1984 Aug. 21. This result refines the preliminary estimate, $-98092 \pm 1$ Hz, reported by Ostro *et al.* (1991).

## DISCUSSION

### *Thermal Inertia and Bulk Density*

Radiometric observations and modeling suggest that the surface of Ra-Shalom has a high thermal inertia, and by inference

is largely bare rock or covered by an extremely thin regolith (Lebofsky *et al.* 1979, Veeder *et al.* 1989, Harris *et al.* 1998). Can the radar data confirm or reject this model? The high end of our radar albedo estimates suggests a dense medium, but using the radar albedo alone to estimate the dielectric constant is misleading in this case because the relatively high circular polarization ratio indicates that a significant amount of the echo is due to "diffuse" scattering. We can, however, make a rough estimate of the echo power that is due solely to single scattering and then use this to infer a dielectric constant, and hence a surface bulk density, as follows.

We adopt a model first proposed by Campbell *et al.* (1993) to interpret linear polarization experiments, modified to deal with our circular polarization experiments. Those authors showed that over a wide range of surface roughness at both C-band (5.6 cm) and L-band (24 cm) wavelengths, the radar cross section from weathered basaltic flows could be modeled as the sum of "small-facet" (SF) and "diffuse" (DIFF) scattering components. The small-facet component contributes singly scattered energy in the form of "expected" polarized OC echoes. The diffuse component contributes equal amounts of energy in both senses of polarization ("expected" and "unexpected" or OC and SC, respectively) due to scattering by wavelength-scale dipole structures and/or multiple scattering. In using this model, we assume no significant returns due to dihedral (double corner-bounce) scattering, "small-perturbation" scattering, or coherent backscattering. Under these assumptions, the small-facet scattering component of the echo is

$$\sigma_{\mathrm{SF}} = \sigma_{\mathrm{OC}} - \sigma_{\mathrm{SC}}, \tag{1}$$

and the fraction of the OC cross section due to small-facet scattering is

$$f_{\mathrm{SF,OC}} = 1 - \mu_{\mathrm{C}}. \tag{2}$$

Since SF scattering contributes only to the OC cross section, the fraction of the total cross section (OC + SC) due to SF scattering is

$$f_{\mathrm{SF}} = (1 - \mu_{\mathrm{C}})/(1 + \mu_{\mathrm{C}}), \tag{3}$$

and that due to diffuse scattering is

$$f_{\mathrm{DIFF}} = 1 - f_{\mathrm{SF}} = 2\mu_{\mathrm{C}}/(1 + \mu_{\mathrm{C}}). \tag{4}$$

Note that the diffuse component for circularly polarized energy in this model could result from wavelength-scale surface structure (i.e., randomly distributed dipoles), multiple scattering, and/or volume scattering; each of these mechanisms has maximum $\mu_{\mathrm{C}} \sim 1$.

Let us assume that these relations hold for disc-integrated observations of Ra-Shalom. The terrestrial observations on which the model is based occurred at intermediate backscattering angles ($\sim$30°–60°). However, there is no evidence that these relationships change with incidence angle, and therefore they should be valid when disc-integrated. Using Eqs. (2) and (3) and Ra-Shalom's observed circular polarization ratio of $0.31 \pm 0.02$, we estimate that 67–71% of the observed OC radar cross section (or 50–55% of the total radar cross section) is due to SF scattering events. Thus the disc-integrated radar albedo due only to SF scattering, $\hat{\sigma}_{\mathrm{SF}}$, satisfies $0.05 \leq \hat{\sigma}_{\mathrm{SF}} \leq 0.23$.

We now use the relation $\hat{\sigma}_{\mathrm{SF}} = gR$ (making the assumption that $\hat{\sigma}_{\mathrm{SF}}$ is the albedo due to Fresnel or "quasi-specular" reflections), where $g$ is the radar backscatter gain and $R$ is the normal Fresnel reflectivity, to estimate the normal reflectivity of Ra-Shalom (Mitchell *et al.* 1996). The gain, $g$, encompasses both the shape of the asteroid and its local surface roughness (i.e., facets). Without any constraints other than the relatively large $\mu_{\mathrm{C}}$, we adopt a range of gains, $1 \leq g \leq 1.5$, and propagate the uncertainties, obtaining $0.03 \leq R \leq 0.23$. An empirical relationship between the bulk density, $d$ (g cm$^{-3}$), and Fresnel reflectivity of geologic material is (Garvin *et al.* 1985)

$$d = 3.2 \ln[(1 + R^{0.5})/(1 - R^{0.5})]. \tag{5}$$

Inserting our interval for $R$ into (5) gives $1.1 \leq d \leq 3.3$ g cm$^{-3}$.

Measurements of the bulk densities of meteorites are scarce, but Consolmagno and Britt (1998) and Britt and Consolmagno (2000) report bulk densities for 14 carbonaceous chondrites, analogues for C-class asteroids, of 1.6–3.4 g cm$^{-3}$, grain densities of 2.43–3.84 g cm$^{-3}$ (reported for only three samples), and porosities (volume fraction of pore space) $\leq$35%. Some of these samples are different fragments of the same meteorite. Our bulk density estimates are consistent with a carbonaceous-chondritic surface with porosity $\leq$70%. Porosities at the upper end of this estimate appear inconsistent with a regolith-free carbonaceous-chondritic surface, but this conclusion rests upon a very limited data set.

Recently, Harris *et al.* (1998) speculated that Ra-Shalom may be an S-class object, based on their estimate of its visual albedo, $p_{\mathrm{v}} = 0.13$, infrared color indices (Veeder *et al.* 1983), and spectral features in the ultraviolet and near-infrared (McFadden *et al.* 1984, 1989). Consolmagno and Britt (1998) also report bulk densities of 18 ordinary chondrites and 7 stony-iron meteorites, both possible analogues for S-class objects, with ranges of 2.95–3.53 and 4.16–4.97 g cm$^{-3}$, respectively. The porosities of all these samples were $\leq$10%. Our estimates of bulk density for Ra-Shalom are inconsistent with a regolith-free stony-iron surface. Stony-iron surfaces with porosities $\sim$20–75% are permitted by our estimates, requiring a thin to substantial regolith if the meteorite porosities reported above are representative. Therefore, our results appear to be consistent with a high surface thermal inertia and stony-iron composition only if Ra-Shalom is near or at the lower end of our effective diameter range.

Our estimates of bulk density for Ra-Shalom are consistent with ordinary-chondritic surfaces with porosities $\leq$70%, and unlike stony-irons, regolith-free chondritic surfaces are permitted. The upper range of allowed porosities requires a substantial

**TABLE VI**
**Spearman's Correlation and Significance Tests**

| Variables | $\rho_{SP}$ | Significance |
|---|---|---|
| $\mu_C$, $\sigma_{TOT}$ | 0.87 | 0.05 |
| $\mu_C$, $\sigma_{SC}$ | 0.90 | 0.04 |
| $\mu_C$, $\sigma_{OC}$ | 0.80 | 0.10 |
| $\mu_C$, $\sigma_{DIFF}$ | 0.90 | 0.04 |
| $\mu_C$, $\sigma_{SF}$ | 0.30 | 0.62 |
| $\mu_C$, BW | 0.30 | 0.62 |
| BW, $\sigma_{TOT}$ | 0.67 | 0.22 |
| BW, $\sigma_{SC}$ | 0.30 | 0.62 |
| BW, $\sigma_{OC}$ | 0.53 | 0.36 |

*Note*. For each pair of variables being tested for correlation, $\rho_{SP}$ is the correlation coefficient, and significance $\leq 0.10$ indicates that we can reject the null hypothesis (no correlation) with 90% confidence. The numbers above represent the least correlative coefficients from any of the tests performed. See text for details.

regolith, and our results are consistent with a high surface thermal inertia and chondritic composition *only* if Ra-Shalom is near the lower end of our effective diameter range.

For discussion purposes, we adopt an optical albedo boundary of $p_v = 0.1$ between S- and C-class asteroids. Using the Bowell *et al.* (1989) relationship between effective diameter and optical albedo, and the absolute magnitude reported for Ra-Shalom (Table I) we find that our estimate $D_{eff}$ 2.4–2.6 km is consistent with an S classification for Ra-Shalom, and that $D_{eff}$ 2.6–3.6 km is consistent with a C classification. Our analyses of Ra-Shalom's bulk density and composition are consistent with these ranges.

### *Correlations in Radar Properties*

Now let us return to the apparent correlations between the values of bandwidth, radar cross section, and circular polarization ratio in Table IV. To assess the significance of these correlations, we use a Spearman rank-order correlation test (Press *et al.* 1989), which allows us to test for correlations without *a priori* assumptions of linearity and is preferred over more traditional correlation tests (e.g., Pearson's) because of the small sample size. Our null hypothesis is that any two variables are uncorrelated, and we adopt a significance level of 10%. (With a sample size of five, the significance resolution of this test is limited; e.g., a 1% significance cannot be meaningfully tested in this case.)

The uncertainties in radar cross section quoted in Table IV are due to random noise and are appropriate (as opposed to the 35% uncertainties in absolute calibration) for comparing daily observations. Even at this reduced level of uncertainty, there is considerable overlap in the radar properties on several days, and Aug. 18 and 21 are virtually indistinguishable. There are larger uncertainties in the rank order of bandwidths, depending on whether one chooses the spectral edges to be at the 1-, 2-, or $3\sigma$ noise level. Because of the limited number of samples (5) and the possible variations in parameter rank order, we adopt the following significance-testing protocol. We ran tests for correlation and significance assuming (1) the current rank order of parameters, (2) reversal of Aug. 18 and 21 in relative rank, and (3) three different bandwidth rankings based on the three spectral edge estimators. We rejected the null hypothesis (variables uncorrelated) only if *all* of these tests attained a significance of 10% or better.

Table VI lists the combinations of variables considered, Spearman correlation coefficient, and significance for the *least* correlative test. There is a significant rank correlation between the polarization ratio and the total, OC, and SC cross sections; in other words, higher radar cross sections are positively and significantly correlated with higher polarization ratios. There is no significant correlation between bandwidth and polarization ratio, contrary to initial impressions, and there is no significant correlation between bandwidth and the total, OC, or SC radar cross sections.

Table VII lists the total radar cross section, circular polarization ratio, fractions of the echo due to SF and DIFF scattering

**TABLE VII**
**Model Scattering Parameters**

| Date | Mean rotational phase (°) | $\mu_C$ | $\sigma_{TOT}$ (km$^2$) | $f_{SF}$ | $f_{DIFF}$ | $\sigma_{SF}$ (km$^2$) | $\sigma_{DIFF}$ (km$^2$) |
|---|---|---|---|---|---|---|---|
| 1984 Aug 18 | 24 | $0.27 \pm 0.02$ | $1.48 \pm 0.03$ | 0.57 | 0.43 | $0.85 \pm 0.03$ | $0.63 \pm 0.02$ |
| 1984 Aug 19 | 104 | $0.35 \pm 0.03$ | $1.82 \pm 0.05$ | 0.48 | 0.52 | $0.88 \pm 0.05$ | $0.94 \pm 0.04$ |
| 1984 Aug 20 | 176 | $0.21 \pm 0.02$ | $1.00 \pm 0.03$ | 0.65 | 0.35 | $0.65 \pm 0.03$ | $0.35 \pm 0.02$ |
| 1984 Aug 21 | 252 | $0.28 \pm 0.02$ | $1.48 \pm 0.04$ | 0.56 | 0.44 | $0.83 \pm 0.03$ | $0.65 \pm 0.03$ |
| 1984 Aug 22 | 328 | $0.38 \pm 0.03$ | $1.74 \pm 0.05$ | 0.45 | 0.55 | $0.78 \pm 0.05$ | $0.96 \pm 0.04$ |

*Note.* Mean rotational phase is the weighted average of all phases observed during the day's observations. $\mu_C$ is the circular polarization ratio. $\sigma_{TOT}$ is the total (OC + SC) radar cross section for the weighted spectral sum of each day's observations. Uncertainties quoted for $\sigma_{OC}$ and $\mu_C$ are $1\sigma$ standard errors caused by background noise. $f_{SF}$ and $f_{DIFF}$ are the model fractions of the radar cross section due to single-facet (SF) scattering and diffuse (DIFF) scattering, respectively. $\sigma_{SF}$ and $\sigma_{DIFF}$ are the model estimates of the radar cross section due to SF and DIFF scattering, respectively; the uncertainties in these estimates are propagated from $\mu_C$ and $\sigma_{TOT}$.

(from Eqs. (3) and (4)), and resulting cross sections due to SF and DIFF scattering. Note the partitioning between SF and DIFF echoes in Table VII; $\sigma_{SF}$ is smaller than $\sigma_{OC}$ and $\sigma_{DIFF}$ is larger than $\sigma_{SC}$ because some of the OC echo is caused by diffuse mechanisms. As a test of the scattering model, there should be little correlation between the polarization ratio and SF cross section: increasing surface roughness should increase the polarization ratio while not significantly affecting the single scattering SF cross section. Increasing wavelength-scale surface roughness should increase the DIFF cross section and result in a high degree of correlation between the polarization ratio and DIFF cross section. Table VI shows that, as expected, there is no significant correlation between the polarization ratio and SF cross section, but a significant correlation between the polarization ratio and DIFF cross section, consistent with terrestrial data (Campbell and Campbell 1992). In other words, the scattering model adopted here appears to correctly separate the SF and DIFF scattered components of the radar cross section.

In Table VII, we note that, although the total radar cross sections vary dramatically from day-to-day, the cross sections due to SF scattering are similar on Aug 18, 19, 21, and 22. This suggests that much of the variation in the total cross section is associated with variation in circular polarization ratio, and by inference, by a rotation-phase-dependent near-surface roughness. The cross-section estimate for Aug 20 is lower than expected, however, and may be caused by large-scale topographic effects on that side ($\sim$180° rotation from the side observed on Aug. 18) of Ra-Shalom.

### *Imminent Opportunities*

The most favorable opportunities for observations of Ra-Shalom in the coming decade occur in 2000 September and 2003 August, both of which support SNRs high enough for radar imaging (daily SNRs of $\sim$200–500 and total SNRs $\sim$1000 on both encounters at Arecibo) and reconstruction of the asteroid's three-dimensional shape at $\sim$100-m resolution (Hudson 1993). In 2000, Ra-Shalom will be $\sim$75° away (measured as an arc along a great circle) from the position of its 1984 closest approach, so the 1984 and 2000 results should yield useful constraints on pole direction.

## ACKNOWLEDGMENTS

M.K.S. gratefully acknowledges a NASA–ASEE summer fellowship (to JPL) and support from NASA and a Bloomsburg University Research and Disciplinary Grant. Part of this research was conducted at the Jet Propulsion Laboratory, operated by the California Institute of Technology under contract with NASA. The Arecibo Observatory is part of the National Astronomy and Ionosphere Center, which is operated by Cornell University under a Cooperative Agreement with the National Science Foundation and with support from NASA. A. W. Harris (DLR), B. Campbell, and an anonymous referee provided excellent reviews.

## REFERENCES

Benner, L. A. M., S. J. Ostro, K. D. Rosema, J. D. Giorgini, D. Choate, R. F. Jurgens, R. Rose, M. A. Slade, M. L. Thomas, R. Winkler, and D. K. Yeomans 1999. Radar observations of Asteroid 7822 (1991 CS). *Icarus* **137**, 247–259.

Bowell, E., B. Hapke, D. Domingue, K. Lumme, J. Peltoniemi, and A. W. Harris 1989. Application of photometric models to asteroids. In *Asteroids II* (R. P. Binzel, T. Gehrels, and M. S. Matthews, Eds.), pp. 524–556. Univ. of Arizona Press, Tucson.

Britt, D. T., and G. J. Consolmagno 2000. The porosity of dark meteorites and structure of low-albedo asteroids. *Icarus* **146**, 213–219.

Campbell, B. A., and D. B. Campbell 1992. Analysis of volcanic surface morphology on Venus from comparison of Arecibo, Magellan, and terrestrial airborne radar data. *J. Geophys. Res.* **97**, 16,293–16,314.

Campbell, B. A., R. E. Arvidson, and M. K. Shepard 1993. Radar polarization properties of volcanic and playa surfaces: Applications to terrestrial remote sensing and Venus data interpretation. *J. Geophys. Res.* **98**, 17,099–17,114.

Chamberlin, A. B., D. K. Yeomans, P. W. Chodas, J. D. Giorgini, R. A. Jacobson, M. S. Keesey, J. H. Lieske, S. J. Ostro, E. M. Standish, and R. N. Wimberly 1997. JPL Solar System dynamics WWW site. *Bull. Am. Astron. Soc.* **29**, 1014. [Abstract]

Consolmagno, G. J., and D. T. Britt 1998. The density and porosity of meteorites from the Vatican collection. *Meteor. Planet. Sci.* **33**, 1231–1241.

Garvin, J. B., J. W. Head, G. H. Pettengill, and S. H. Zisk 1985. Venus global radar reflectivity and correlations with elevation. *J. Geophys. Res.* **90**, 6859–6871.

Harris, A. W., J. K. Davies, and S. F. Green 1998. Thermal infrared spectrophotometry of the near-Earth asteroids 2100 Ra-Shalom and 1991 EE. *Icarus* **135**, 441–450.

Helin, E. F., E. M. Shoemaker, and R. F. Wolfe 1978. Ra-Shalom: Third member of the Aten class of Earth-crossing asteroids. *Bull. Am. Astron. Soc.* **10**, 732.

Hudson, R. S., and S. J. Ostro 1999. Physical model of Asteroid 1620 Geographos from radar and optical data. *Icarus* **140**, 369–378.

Hudson, S. 1993. Three-dimensional reconstruction of asteroids from radar observations. *Remote Sens. Rev.* **8**, 195–203.

Lebofsky, L. A., M. J. Lebofsky, and G. H. Rieke 1979. Radiometry and surface properties of Apollo, Amor, and Aten asteroids. *Astron. J.* **84**, 885–888.

Lebofsky, L. A., and J. R. Spencer 1989. Radiometry and thermal modeling of asteroids. In *Asteroids II* (R. P. Binzel, T. Gehrels, and M. S. Matthews, Eds.), pp. 128–147. Univ. of Arizona Press, Tucson.

Magri, C., S. J. Ostro, K. D. Rosema, M. L. Thomas, D. L. Mitchell, D. B. Campbell, J. F. Chandler, I. I. Shapiro, J. D. Giorgini, and D. K. Yeomans 1999. Mainbelt asteroids: Results of Arecibo and Goldstone radar observations of 37 objects during 1980–1995. *Icarus* **140**, 379–407.

McFadden, L. A., M. J. Gaffey, and T. B. McCord 1984. Mineralogical–petrological characterization of near-Earth asteroids. *Icarus* **59**, 25–40.

McFadden, L. A., D. J. Tholen, and G. J. Veeder 1989. Physical properties of Aten, Apollo, and Amor asteroids. In *Asteroids II* (R. P. Binzel, T. Gehrels, and M. S. Matthews, Eds.), pp. 442–467. Univ. of Arizona Press, Tucson.

Mitchell, D. L., S. J. Ostro, R. S. Hudson, K. D. Rosema, D. B. Campbell, R. Velez, J. F. Chandler, I. I. Shapiro, J. D. Giorgini, and D. K. Yeomans 1996. Radar observations of Asteroids 1 Ceres, 2 Pallas, and 4 Vesta. *Icarus* **124**, 113–133.

Mitchell, D. L., S. J. Ostro, K. D. Rosema, R. S. Hudson, D. B. Campbell, J. F. Chandler, and I. I. Shapiro 1995. Radar observations of Asteroids 7 Iris, 9 Metis, 12 Victoria, 216 Kleopatra, and 654 Zelinda. *Icarus* **118**, 105–131.

Ostro, S. J., D. B. Campbell, J. F. Chandler, I. I. Shapiro, A. A. Hine, R. Velez, R. F. Jurgens, K. D. Rosema, R. Winkler, and D. K. Yeomans 1991. Asteroid radar astrometry. *Astron. J.* **102**, 1490–1502.

Ostro, S. J., R. Connelly, and L. Belkora 1988. Asteroid shapes from radar echo spectra: A new theoretical approach. *Icarus* **73**, 15–24.

Ostro, S. J., A. W. Harris, D. B. Campbell, I. I. Shapiro, and J. W. Young 1984. Radar and photoelectric observations of Asteroid 2100 Ra-Shalom. *Icarus* **60**, 391–403.

Ostro, S. J., K. D. Rosema, and R. F. Jurgens 1990. The shape of Eros. *Icarus* **84**, 334–351.

Pravec, P., M. Wolf, and L. Sarounova 1998. Lightcurves of 26 near-Earth asteroids. *Icarus* **136**, 124–153.

Press, W. H., B. P. Flannery, S. A. Teukolsky, and W. T. Vetterling 1989. *Numerical Recipes: The Art of Scientific Computing*. Cambridge Univ. Press, Cambridge.

Tedesco, E. F., D. L. Matson, and G. J. Veeder 1984. Classification of IRAS asteroids. In *Asteroids II* (R. P. Binzel, T. Gehrels, and M. S. Matthews, Eds.), pp. 290–297. Univ. of Arizona Press, Tucson.

Tholen, D. J., and M. A. Barucci 1984. Asteroid taxonomy. In *Asteroids II* (R. P. Binzel, T. Gehrels, and M. S. Matthews, Eds.), pp. 298–315. Univ. of Arizona Press, Tucson.

Veeder, G. J., M. S. Hanner, D. L. Matson, E. F. Tedesco, L. A. Lebofsky, and A. T. Tokunaga 1989. Radiometry of near-Earth asteroids. *Astron. J.* **97**, 1211–1219.

Veeder, G. J., D. L. Matson, G. Hoover, and C. Kowal 1983. Infrared (JHK) photometry of asteroids. II. *Astron. J.* **88**, 1060–1063.